ELSEVIER

Journal of Organometallic Chemistry 568 (1998) 63–76

Journal of Organometallic Chemistry

Ligand additivity in 47-electron clusters. Electrochemistry of $(\mu\text{-H})Ru_3(\mu_3\text{-}\eta^3\text{-XCCRCR}')(CO)_{9-n}(PPh_3)_n$ and reactions with electrophiles: one-electron oxidation and adduct formation

Huirong Yao [a], Robert D. McCargar [a], Robert D. Allendoerfer [a], Jerome B. Keister [a,*], Arthur A. Low [b]

[a] *Department of Chemistry, University at Buffalo, State University of New York, Buffalo, NY 14260-3000, USA*
[b] *Department of Chemistry, Tarleton State University, Stephenville, TX 76402, USA*

Received 10 February 1998; received in revised form 11 May 1998

Abstract

Reactions of clusters $HRu_3(\mu_3\text{-}\eta^3\text{-XCCRCR}')(CO)_{9-n}(PPh_3)_n$ (X = OMe, R = R′ = Me, $n = 1, 2, 3$; X = MeO, R = H, R′ = EtO, $n = 2, 3$; X = Et_2N, R = H, R′ = Me, $n = 1, 2$) with electrophilic reagents proceed either by 1-electron transfer or by Lewis acid-base adduct formation. The HOMO for the cluster series is Ru–Ru bonding with contributions from all three Ru atoms. Cyclic voltammograms of $HRu_3(\mu_3\text{-}\eta^3\text{-XCCRCR}')(CO)_{9-n}(PPh_3)_n$ ($n = 2, 3$) display in each case an electrochemically reversible to quasi-reversible, 1-electron oxidation, followed by an irreversible, 1-electron oxidation at a significantly more positive potential. The potential for the first oxidation is lowered both by an increasing degree of PPh_3 substitution and an increasing pi donor capability of the allylidene substituents. The dependence of the oxidation potential upon substitution of the metal and carbon framework atoms is analyzed as an example of ligand additivity in cluster systems. Radical cations derived from the di- and tri-substituted 1,3-dimetalloallyl clusters can be generated by oxidation with tris(4-bromophenyl)aminium hexachloroantimonate. These radical cations decompose within a few minutes at room temperature but are stable for long periods at temperatures below −40°C. Electrophilic addition of $E = H^{1+}$, Ag^{1+} or $Au(PPh_3)^{1+}$ to the Ru–Ru bonds is observed. Adducts $[ERu_3H(\mu_3\text{-}\eta^3\text{-XCCRCR}')(CO)_{9-n}(PPh_3)_n]^{1+}$ have been characterized by IR and ^1H- and ^{31}P-NMR spectroscopies. The $Au(PPh_3)$ moiety is found to bridge two or three Ru–Ru bonds in these adducts. Substitutional isomerism is induced by electrophilic addition.

Keywords: Ruthenium; Cyclic voltammetry; Electrochemistry; Metal clusters; Allylidene derivatives

1. Introduction

The importance of odd-electron intermediates in organometallic chemistry is now well-recognized [1]. Electrochemical activation of organometallic compounds has been used to induce such reactions as ligand substitution, insertion, isomerization, oxidative addition and reductive elimination. Both 19- and 17-electron monometallic intermediates are involved in these processes. Oxidations of 18-electron monometallic complexes generate 17-electron species in which the unpaired electron is in an orbital which is largely of metal d character. Polymetallic cluster radical species are also very reactive but the description of the singly occupied molecular orbital (SOMO) is different between the higher and lower oxidation states in most cases. Since the HOMOs of most saturated metal carbonyl clusters have metal-metal bonding character, 1-electron oxidations generate radicals in which the SOMO is metal-metal bonding and may be delocalized over several metal atoms.

* Corresponding author. Tel.: +1 716 6456800; fax: +1 716 6456963.

0022-328X/98/$19.00
PII S0022-328X(98)00795-5

In this work, we report on the electrochemistry of the clusters HRu_3 (μ_3-η^3-XCCRCR′)$(CO)_{9-n}(PPh_3)_n$ (X = OMe, R = R′ = Me, $n = 1–3$; X = NEt_2, R = H, R′ = Me, $n = 1, 2$; X = OMe, R = H, R′ = OEt, $n = 2, 3$) (Fig. 1) and also their reactivities toward electrophile/oxidants. Since the HOMOs for these clusters are metal–metal bonding in character and involve all three metal atoms, we were interested in the comparison of the reactivity of this cluster class with the reactivities previously established for $H_3Ru_3(\mu_3\text{-}CX)(CO)_{9-n}L_n$ [2], for which the HOMO is metal–carbon bonding in character, and $H_2Ru_3(\mu_3\text{-}\eta^2\text{-}XCCR)(CO)_{9-n}(PPh_3)_n$ [3] for which the HOMO is also metal-metal bonding in character but is localized primarily on two of the three Ru atoms. Another point of interest was to determine the effects of ligand and hydrocarbyl substitution upon the HOMO energy. This cluster series provides an unusual opportunity to make systematic changes in the substituents on organometallic cluster core and thereby to 'tune' the oxidation potential of the cluster. The $HRu_2(XCCRCR')^{2-}$ unit is isolobal with the cyclopentadienyl anion, implying an analogy between these clusters and the half-sandwich complex $[CpRu(CO)_3]^+$. It has been noted that increasing pi donor ability of the hydrocarbyl substituents causes lengthening of the Ru–CX bond length of the 1,3-dimetalloallyl clusters in what was termed a nido-arachno polyhedral distortion [4,5]. A similar distortion had been observed for $(C_5H_4NEt_2)Fe(CO)\{PPh(OEt)_2\}Br$ [6], thus supporting the isolobal analogy between $XCC_4H_4^{1-}$ and $HRu_2(XCCRCR')^{2-}$.

A preliminary account of some of these results has appeared [7].

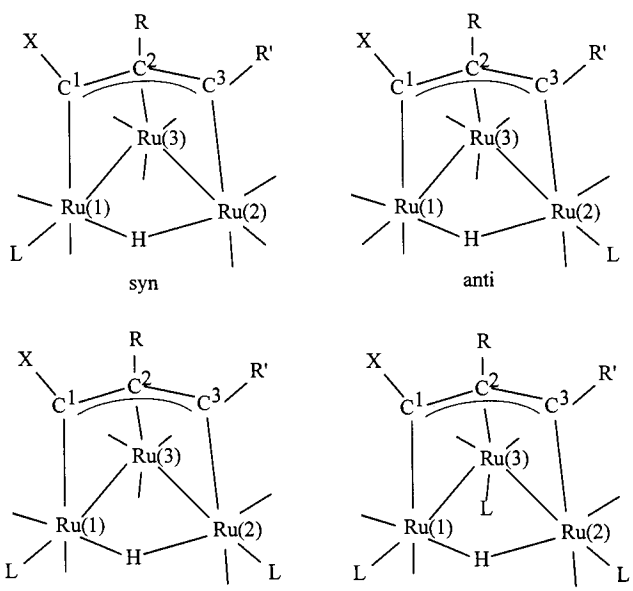

Fig. 1. Structures of $HRu_3(\mu_3\text{-}\eta^3\text{-}XCCRCR')(CO)_{9-n}(PPh_3)_n$ with numbering scheme for metal atoms and carbon atoms.

2. Experimental section

2.1. General

All reactions were carried out using standard Schlenk techniques. Dichloromethane was distilled from calcium hydride before use. All other solvents used were of reagent grade quality and were not purified unless otherwise noted. Silver trifluoromethanesulfonate, tris(4-bromophenyl)aminium hexachloroantimonate ('magic blue'), and trifluoroacetic acid were used as received from Aldrich. $AuPPh_3Cl$ [8] and $(\mu\text{-}H)Ru_3(\mu_3\text{-}\eta^3\text{-}XCCRCR')(CO)_{9-n}(PPh_3)_n$ (X = OMe, R = R′ = Me, $n = 1–3$; X = NEt_2, R = H, R′ = Me, $n = 1, 2$; X = OMe, R = H, R′ = OEt, $n = 2, 3$) [5] were synthesized according to previously reported procedures.

Infrared spectra were recorded on a Mattson Instruments Alpha Centauri FTIR spectrometer, fitted with a Beckman VLT-2 variable temperature unit when low temperature was required in recording the spectra of radicals, a Nicolet Magna 550 spectrophotometer, or a Beckman 4250 spectrophotometer.

^{1}H-NMR spectra were obtained on JEOL FX-90, Varian Associates Gemini 300, or Varian Associates VXR-400S instruments, using deuterochloroform as solvent and TMS as reference. ^{31}P-NMR spectra were recorded on the VXR-400S instrument in deuterochloroform and chemical shifts are reported relative to *o*-phosphoric acid. The selective phosphorus decoupling ^{1}H-NMR spectroscopy was performed at Varian-Florham Park on a Varian Unity$^+$ 500 MHz instrument in d_2-dichloromethane.

EPR spectra were recorded on an IBM/Bruker X-band ER200 SRC spectrometer, with a microwave power of 20 mW, in dichloromethane solution at 225 or 125 K.

Mass spectra (FAB) were obtained with a VG 70-SE spectrometer.

2.2. $[HRu_3(\mu_3\text{-}\eta^3\text{-}MeOCCMeCMe)(CO)_7(PPh_3)_2(AuPPh_3)][SO_3CF_3]$

To a 100 ml Schlenk flask was added $HRu_3(\mu_3\text{-}\eta^3\text{-}MeOCCMeCMe)(CO)_7(PPh_3)_2$ (61 mg, 0.054 mmol) and dichloromethane (15 ml) under nitrogen. In a separate 50 ml Schlenk flask was placed $Au(PPh_3)Cl$ (32 mg, 0.066 mmol) and $AgSO_3CF_3$ (17 mg, 0.065 mmol) in dichloromethane; the mixture was stirred for 10 min under nitrogen to allow complete precipitation of AgCl. The solution was then passed through a 60 ml coarse frit into the cluster solution. Over a period of 10 min the solution went from red-orange to deep purple in color. An IR spectrum was taken after 30 min and it was observed that the starting material had completely

disappeared. The NMR spectra initially showed only one isomer (isomer I); however, after 24 h a 40:10:50 mixture of isomers I, II, and III was noted. The reaction was stirred overnight to ensure complete reaction. The solvent was removed and the resulting solid was recrystallized from dichloromethane/cyclohexane (1:1) to give a dark purple powder (46.9 mg, 49.8%).

$[HRu_3(\mu_3\text{-}\eta^3\text{-MeOCCMeCMe})(CO)_7(PPh_3)_2(AuPPh_3)][SO_3CF_3]$: Anal. Calc. for $AuC_{68}H_{55}F_3O_{11}P_3Ru_3S$: C, 47.20; H, 3.20. Found: C, 46.45; H, 3.27. IR (CH_2Cl_2, cm^{-1}): 2065 (s), 2022 (vs), and 1983 (m,br). ^{1}H-NMR ($CDCl_3$, ppm): isomer I, 7.2 (m, 45H), 3.03 (s, 3H), 2.28 (s, 3H), 2.10 (d, 3H, $J_{PH} = 3.3$ Hz), −18.96 (t, 1H, $J_{PH} = 12.0$ Hz); isomer II, 3.65 (s, 3H), 1.90 (s, 3H), 1.51 (d, 3H, $J_{PH} = 5.0$ Hz), and −20.90 (d, 1H, $J_{PH} = 14.0$ Hz); isomer III, 2.92 (s, H), 2.00 (s, 3H), 1.60 (s, 3H), and −21.00 (d, 1H, $J_{PH} = 16.2$ Hz). ^{31}P{^{1}H}-NMR ($CDCl_3$, ppm): isomer I, 62.3 (dd, $1P_A$), 47.7 (dd, $1P_B$), and 45.5 (dd, $1P_C$), $J_{AB} = 30.0$ Hz, $J_{AC} = 20.0$ Hz, and $J_{BC} = 10.0$ Hz; isomer II, 61.9(t), $J_{PP} = 10.0$ Hz (other resonances were likely obscured by those due to isomers I and III); isomer III, 66.7 (t, $1P_A$), 47.3 (dd, $1P_B$), and 43.5 (dd, $1P_C$), $J_{AB} = J_{AC} = 20.0$ Hz, $J_{BC} = 10.0$ Hz.

2.3. $[HRu_3(\mu_3\text{-}\eta^3\text{-}NEt_2CCHCMe)(CO)_7(PPh_3)_2(AuPPh_3)][SO_3CF_3]$

The product was prepared by using the procedure described above. Recrystallization of the red solid from dichloromethane/cyclohexane (1:1) gave a red-orange powder (56.2 mg, 98.5%).

$[HRu_3(\mu_3\text{-}\eta^3\text{-}NEt_2CCHCMe)(CO)_7(PPh_3)_2(AuPPh_3)][SO_3CF_3]$: Anal. Calc. for $AuC_{70}H_{60}F_3NO_{10}P_3Ru_3S$: C, 47.84.; H, 3.44. Found: C, 48.21; H, 3.29. IR (CH_2Cl_2, cm^{-1}): 2049 (s), 2013 (vs), and 1966(m,br). ^{1}H-NMR ($CDCl_3$, ppm): 7.3 (m, 45H), 6.82 (d, $1H_A$, J_{AB} 2.5 Hz), 4.10 (dq, 1H, J_{HH} 14, 7 Hz), 3.97 (dq, 1H, J_{HH} 14, 7 Hz), 3.61 (dq, 1H, J_{HH} 14, 7 Hz), 3.34 (dq, 1H, J_{HH} 14, 7 Hz), 2.51(d, 3H, $J_{P(B)H}$ 3.2 Hz), 1.64 (t, 3H, J_{HH} 7 Hz), 0.84 (t, 3H, J_{HH} 7 Hz), and −16.85 (dt, $1H_B$, J_{PH} 12.1, J_{AB} 2.5 Hz). ^{31}P{^{1}H}-NMR ($CDCl_3$, ppm): 60.2 (d, $1P_A$), 41.2 (d, $1P_B$), and 37.2 (s, $1P_C$), $J_{AB} = 30.0$ Hz.

2.4. $[HRu_3(\mu_3\text{-}\eta^3\text{-}MeOCC_2Me_2)(CO)_6(PPh_3)_3(AuPPh_3)][SO_3CF_3]$

The product was prepared by using the procedure described above for $[HRu_3(\mu_3\text{-}\eta^3\text{-MeOCCMeCMe})(CO)_7(PPh_3)_2(AuPPh_3)][SO_3CF_3]$. Recrystallization from dichloromethane/hexane (1:1) gave a dark purple power (95%).

$[HRu_3(\mu_3\text{-}\eta^3\text{-}MeOCC_2Me_2)(CO)_6(PPh_3)_3(AuPPh_3)][SO_3CF_3]$: IR ($CH_2Cl_2$, cm^{-1}): 2025 (vs), 2009 (vs), 1986 (s), 1966 (w) cm^{-1}. ^{1}H-NMR ($CDCl_3$, ppm): 7.3 (m, 60H), 3.12 (s, 3H), 1.87 (s, 3H), 1.27 (d, 3H, $J_{PH} = 3.6$ Hz), −18.98 (t, 1H, $J_{PH} = 11.8$ Hz). ^{31}P{^{1}H}-NMR ($CDCl_3$, ppm): 58.66 (ddd, $1P_A$, $J_{AC} = 27$ Hz, $J_{PP} = 19$, 17 Hz), 48.5 (m, $1P_B$), 45.1 (ddd, $1P_C$, $J_{AC} = 27$ Hz, $J_{PP} = 14$, 12 Hz), 38.9 (m, $1P_D$).

2.5. $HRu_3(\mu_3\text{-}\eta^3\text{-}MeOCCMeCMe)(CO)_7(PPh_3)_2(AgSO_3CF_3)$

Addition of one equivalent of $AgSO_3CF_3$ to a dichloromethane solution of $HRu_3(\mu_3\text{-}\eta^3\text{-MeOCCMeCMe})(CO)_7(PPh_3)_2$ resulted in an immediate color change to dark red. The solvent was removed by rotoevaporation to give a dark purple powder. The product was characterized by NMR spectroscopy. The solution IR spectrum could not be obtained, only bands due to the starting material were present. This is perhaps due to reaction with the window material.

$HRu_3(\mu_3\text{-}\eta^3\text{-MeOCCMeCMe})(CO)_7(PPh_3)_2(AgSO_3CF_3)$. ^{1}H-NMR ($CDCl_3$, ppm): 7.1 (m, 30H), 2.98 (s, 3H), 2.24 (s, 3H), 2.03 (d, 3H, $J_{PH} = 2.4$ Hz), and −19.21 (t, 1H, $J_{PH} = 12.2$ Hz). ^{31}P{^{1}H}-NMR ($CDCl_3$, ppm): 45.8 (s, 1P) and 42.2 (s, 1P).

2.6. $[H_2Ru_3(\mu_3\text{-}\eta^3\text{-}MeOCC_2Me_2)(CO)_7(PPh_3)_2][O_2CCF_3]$

To a solution of 40 mg $HRu_3(\mu_3\text{-}\eta^3\text{-}MeOCC_2Me_2)(CO)_7(PPh_3)_2$ in $CDCl_3$ (0.6 ml) in an NMR tube was added 8–10 μl of trifluoroacetic acid. The NMR tube was shaken vigorously, and the spectrum was taken immediately. No reaction was observed initially. After 2 h the product (isomer I) was characterized as the protonated cluster by its ^{1}H-NMR spectrum. After standing overnight a minor protonated product (isomer II) appeared with a ratio of 1:3 to isomer I. The final ratio of the products is 1:2 after 2 days.

The rate of the protonation can be increased by adding more acid. The color of the solution changed from orange to dark red rapidly. However, in addition to isomer I an unknown product characterized by a doublet at −14.19 ppm ($J = 8.4$ Hz) was observed in the ^{1}H-NMR spectrum.

$[H_2Ru_3(\mu_3\text{-}\eta^3\text{-}MeOCC_2Me_2)(CO)_7(PPh_3)_2][O_2CCF_3]$: IR ($CH_2Cl_2$, cm^{-1}): 2135 (w), 2072 (s), 2041 (vs), 2010 (m), 1999(w), 1971 (w). ^{1}H-NMR ($CDCl_3$, ppm): 7.3 (m, 30H), isomer I, 4.00 (s, 3H), 1.78 (s, 3H), 1.45 (d, $J_{PH} = 2.8$ Hz), −14.40 (ddd, 1H, $J_{PH} = 19.2$ Hz, 10.0 Hz, $J_{HH} = 2$ Hz), −18.20 (dt, 1H, $J_{PH} = 17.6$ Hz, 2 Hz, $J_{HH} = 2$ Hz); isomer II, 3.17 (s, 3H), 2.31 (s, 3H), 2.01 (s, 3H), −15.14 (ddd, 1H, $J_{PH} = 13.2$ Hz, 7.6 Hz,

$J_{HH} = 2$ Hz), −18.45 (dt, 1H, $J_{PH} = 16.8$ Hz, 2 Hz, $J_{HH} = 2$ Hz). $^{31}P\{^1H\}$-NMR ($CDCl_3$, ppm): isomer I, 37.6 (s, br, 1P), 34.1 (s, br, 1P); isomer II, 42.5 (s, br, 1H), 29.0 (s, br, 1H).

2.7. $[H_2Ru_3(\mu_3\text{-}\eta^3\text{-}Et_2NCCHCMe)(CO)_7(PPh_3)_2][O_2CCF_3]$

The reaction was performed in an NMR tube. To a solution of $HRu_3(Et_2NCCHCMe)(CO)_7(PPh_3)_2$ in $CDCl_3$ was added 2–3 μl trifluoroacetic acid. The solution was shaken vigorously, and the color turned to yellow-green immediately. The product was characterized by spectroscopic methods.

$[H_2Ru_3(\mu_3\text{-}\eta^3\text{-}Et_2NCCHCMe)(CO)_7(PPh_3)_2][O_2CCF_3]$: IR ($CH_2Cl_2$, cm^{-1}): 2085 (vs), 2055 (m), 2040 (s), 2005 (sh), 1973 (w). ^{1}H-NMR ($CDCl_3$, ppm): 7.3 (m, 45H), 6.72 (s, 1H), 4.01 (dq, 1H, $J_{HH} = 10$, 7 Hz), 3.97 (dq, 1H, $J_{HH} = 10$, 7 Hz), 3.66 (dq, 1H, $J_{HH} = 10$, 7 Hz), 3.44 (dq, 1H, $J_{HH} = 10$, 7 Hz), 2.79 (d, 3H, $J_{PH} = 2.4$ Hz), 1.58 (t, 3H, $J_{HH} = 7$ Hz), 0.85 (t, 3H, $J_{HH} = 7$ Hz), −14.56 (dd, 1H, $J_{PH} = 20.8$ Hz, $J_{HH} = 2$ Hz) and −16.73 (dt, 1H, $J_{P(1)H} = J_{P(2)H} = 12.2$ Hz, $J_{HH} = 2$ Hz). $^{31}P\{^1H\}$-NMR ($CDCl_3$, ppm): 34.8 (s, br, 1P), 33.6 (s, br, 1P); selective proton decoupling of the phenyl region revealed that the resonance at 34.8 ppm was coupled with both hydride resonances ($J_{P-H} = 21$ and 12 Hz).

2.8. Electrochemistry

All the voltammetric experiments were performed with a BAS-100 electrochemical analyzer using conventional three-electrode arrangements. Temperature was controlled at 25 ± 1°C by using a Fisher (model 90) refrigerator. Tetrabutylammonium tetrafluoroborate (TBATFB) electrolyte was prepared from tetrabutylammonium bromide and tetrafluoroboric acid, recrystallized from ethyl acetate-pentane twice, and dried in vacuo. The solutions in the electrochemical cell were saturated with nitrogen between measurements.

The working electrode was either a platinum (homemade) or carbon (BAS) disk. The areas of the working electrodes were measured as 0.024 (Pt) and 0.073 (carbon) $\pm$ 0.001 cm^2 by application of the Cottrell equation to the limiting current using these electrodes in 0.001 M $K_4Fe(CN)_6 \cdot 3H_2O$ in aqueous 0.1 M KCl. The concentration of the analytes was 10^{-3} M, while the electrolyte was 0.1 M TBATFB in dichloromethane. The auxiliary electrode was a platinum wire and the pseudo-reference electrode was a silver wire. Compensation for iR drop was employed (about 98% compensated). The scan rates of 50–800 mV s^{-1} were used in cyclic voltammetry (CV). All the potentials measured by cyclic voltammetry are referenced to the ferrocene/ferrocenium couple under the same conditions (ferrocene displays a 'reversible' cyclic voltammogram at $E_{1/2}$ 0 mV, $\Delta E_p = 72$ mV at a scan rate of 100 mV s^{-1}). The $E_{1/2}$ for the ferrocene/ferrocenium couple is assumed to be 0.665 V versus the NHE. Peak current ratios were calculated using the equation [9]:

$$i_{p,c}/i_{p,a} = (i_{p,c})_0/i_{p,a} + 0.485(i_{sp})_0/i_{p,a} + 0.086$$

where the $i_{p,c}$ is the cathodic peak current, $i_{p,a}$ is the anodic peak current, $(i_{p,c})_0$ is the uncorrected cathodic current, and $(i_{sp})_0$ is the uncorrected peak current at the switching potential.

For controlled potential coulometry, the coulometric cell was assembled as follows: To a jacketed cell, kept at constant temperature (−20°C) by circulated fluid from a HAKKE D8-GH refrigerated bath/circulator, was added 25 ml of a 0.1 M TBATFB solution in dichloromethane and 6.6 mg (5.78×10^{-6} mol) of $HRu_3(Et_2NCCHCMe)(CO)_7(PPh_3)_2$. A silver wire was used as a pseudo-reference electrode, and a platinum wire in a fritted disk was used as an auxiliary electrode. The working electrode was a platinum gauze electrode (Aesar Unimesh, gauze type 39/1, 25 mm diameter × 50 mm height cylinder), placed directly into the solution. A cyclic voltammogram was performed prior to the coulometry to determine the potential for electrolysis. The solution was stirred and purged with nitrogen while the experiment was performed. After 140 min the current had decayed to background levels and the experiment was halted. The amount of net charge passed was 0.577 C, corresponding to $n = 1.03$.

Normal pulse voltammograms (NPV) at pulse widths of t_p 60–200 ms, were recorded. The diffusion coefficient D_R for each cluster compound was determined by the analysis of the limiting currents in NPV by linear regression in terms of the Cottrell equation.

2.9. Chemical oxidations and subsequent reactions

For the clusters $HRu_3(XCCRCR')(CO)_{9-n}(PPh_3)_n$ (X = OMe, R = Me, R′ = Me, $n = 2$, 3; X = OMe, R = H, R′ = OEt, $n = 2$, 3; X = NEt_2, R = H, R′ = Me, $n = 2$), the oxidation reactions were conducted in dichloromethane in a Schlenk flask under nitrogen, unless otherwise noted. The oxidant (usually one equivalent) was added as a solid to a solution of the cluster. The reaction mixture was stirred for about 1 min before spectroscopic measurements.

Low temperature IR spectra were recorded by using a Beckman VLT-2 variable temperature IR cell, which was cooled by a chlorobenzene slush. A freshly distilled dichloromethane solution of the cluster (ca. 5×10^{-3} M) was mixed with one equivalent or more of 'magic blue', depending on the cluster, and added quickly with a syringe. The spectra of the clusters were recorded at

Table 1
Infrared spectra of $[HRu_3(XCCRCR')(CO)_{9-n}(PPh_3)_n]^{1+}$ and decomposition products in dichloromethane

Cluster	ν (CO) cm^{-1}			
	Before oxidation	5 mins at −40°C	1 h or more at −40°C	Decomposition at 25°C
X = NEt_2, R = H, R′ = Me, $n = 2$	2035 (s), 1992 (s), 1959 (w), 1950 (w)	2092 (vs), 2066 (m), 2048 (m), 2033 (s), 2005 (w), 1988 (m), 1956 (w)	2066 (w), 2033 (s), 2006 (s), 1956 (m)	
X = OMe, R = R′ = Me, $n = 2$	2040 (s), 2002 (s), 1962 (w), 1972 (m)	2075 (sh), 2064 (s), 1972 (m), 2005 (s), 1960 (w)	2068 (s), 2033 (m), 2003.9 (s)	2075.7 (vs), 2061.3 (sh), 2014.0 (s), 1982.2 (sh, m)
X = OMe, R = R′ = Me, $n = 3$	2013 (s), 1988 (m), 1955 (m)	2062 (s), 2045 (s), 2008 (vs, br), 1974 (sh), 1959 (m)	2068 (sh), 2058 (s), 2004 (vs)	2074.3 (vs), 2060.6 (sh), 2014.5 (s), 1976.0 (m)
X = OMe, R = H, R′ = OEt, $n = 2$	2042 (s), 2001 (s), 1966 (w)	2068 (s), 2033 (m), 2004 (s), 1966 (w)	2068 (s), 2006 (s), 1961 (s)	2082.0 (s), 2069.5 (s), 2026.1 (m), 2014.5 (sh)
X = OMe, R = H, R′ = Et, $n = 3$	2017 (vs), 1995 (m), 1958 (m)	2080 (sh), 2068 (vs), 2046 (m), 2021 (s), 2005 (s, br), 1980 (m, br)	2080 (sh), 2068 (s), 2008(s, br), 1967 (m, br)	2081.1 (s), 2068.5 (s), 2032.2 (sh), 2015.5 (m)

−45°C periodically for at least 1 h, at 5–10 min time intervals.

The reduction of the $[HRu_3(Et_2NCCHCMe)(CO)_7(PPh_3)_2]^{1+}$ was conducted at −45°C with the solution cooled in a chlorobenzene slush bath. About one equivalent of $HSn(C_4H_9)_3$ was added to the dark green solution. The color of the solution turned to dark red slowly upon shaking under nitrogen, and the IR spectrum was taken after 15 min.

Unlike the slow decomposition of the cluster radicals at low temperature, the IR spectrum of the decomposition product(s) of each radical cluster at room temperature appeared fairly clean, except for the product derived from $[HRu_3(Et_2NCCHCMe)(CO)_7(PPh_3)_2]^{1+}$. The IR spectral data of the CO stretching frequencies are listed in Table 1. Based upon the similarity of the spectra arising from decomposition of di- and trisubstituted derivatives having the same allylidene ligand, it is probable that the major carbonyl-containing decomposition products of the di-substituted and the tri-substituted cluster cations are the same.

The only product which was identified by spectroscopic methods was derived from decomposition of $[HRu_3(MeOCCHCOEt)(CO)_7(PPh_3)_2]^{1+}$. ^1H- and ^{31}P-NMR spectra showed only one significant product, proposed to be $[(\mu\text{-H})Ru_2(\mu\text{-Cl})(MeOCCHCOEt)(CO)_3(PPh_3)_2]^{1+}$. In the ^1H-NMR spectrum, resonances due to a hydride bridging a $Ph_3PRuRuPPh_3$ edge (−11.74 ppm (td, $J_{P(1)-H} \sim J_{P(2)-H} = 10.2$, J_{H-H} 1.6 Hz)) and to the MeOCCHCOEt moiety are noted. The $^{31}P\{^1H\}$-NMR spectrum displays two singlets at 44.8 and 45.0 ppm. The mass spectrum displays a molecular ion at m/z 961, the mass envelope of which matches that calculated for the formula $[C_{49}ClH_{40}P_2O_9Ru_3]^{1+}$.

2.10. Low temperature EPR spectra

A specially designed reactor with a quartz EPR tube was used for the oxidation reaction and the EPR analysis. Equivalent amounts of reactants, cluster and 'magic blue', were placed in separate side-arms. The reactor was evacuated and the solvent dichloromethane was degassed by more than three freeze (liquid nitrogen)–pump–thaw (dry ice/acetone) cycles. The solvent was vacuum transferred into both sidearms. After the materials in the side-arms were completely dissolved, the 'magic blue' solution was quickly poured into the cluster solution, and the mixture (ca. 4×10^{-3} M) was shaken for ca. 1 min before it was transferred in the neighboring EPR tube. The EPR tube was kept frozen until it was allowed to warm up in a dry ice/acetone bath for spectroscopic measurements. The EPR spectrometer probe was cooled down by a flow of cold nitrogen gas and the temperature was controlled a thermostat saturated with nitrogen gas. The spectrum in the frozen solution of dichloromethane (125 K) was taken at first. The spectrometer was gradually warmed up to 225 K and the spectrum in solution was recorded. The freeze–thaw process was repeated.

2.11. Data analysis of ligand and substituent effects

Non-linear least squares fits of the oxidation potentials to Eq. (1) were performed with the Marquardt–Levenburg method using the program PSI-Plot (Poly Software International). Error limits for the parameters are the standard deviations.

2.12. Molecular orbital calculations

Fenske–Hall molecular orbital calculations [10] were performed on the clusters (μ-H)Ru_3(μ_3-XCCRCR′)$(CO)_9$ (X = Me, R = R′ = Me; X = OMe, R = R′ = Me; X = NMe_2, R = H, R′ = Me) in their experimentally determined structures.[4,11] The ruthenium basis functions were taken from Richardson et al. [12] The carbon, nitrogen, oxygen and hydrogen functions were taken from the double-H functions of Clementi [13] and reduced to a single-H function [14] except for the atom's valence orbitals which were retained as the double-H function. The atomic functions were made orthogonal by the Schmidt procedure. The percent atomic contributions to the HOMO and LUMO were obtained from the eigenvectors of the respective orbitals.

3. Results

3.1. Bonding

The Ru_3C_3 cluster core can be described as a pentagonal pyramid with one apical and two basal Ru atoms and three basal carbon atoms, an arachno structure according to the polyhedral skeletal electron pair theory. The bonding of the allylidene fragment to the trimetallic framework can also be described as involving two sigma Ru–C bonds to the 'basal' Ru atoms and one η^3-π-bond to the 'apical' Ru atom. The allylidene ligand has been considered a 5-electron, neutral donor, and the Ru–H–Ru bond can be treated as a 3-center-2-electron bond.

A previous study of (μ-H)Ru_3(μ_3-η^3-MeCCHCMe)$(CO)_9$, by using UV photoelectron spectroscopy, coupled with CNDO quantum-mechanical calculations, found that the HOMO is metal-metal bonding in character [11]. The two highest energy occupied MOs, nearly degenerate (-7.14 and -7.22 eV), were comprised of 45% (both) basal Ru/23% apical Ru and 47% (both) basal Ru/35% apical Ru, respectively. At least with respect to the HOMO it would be expected that PR_3 substitution on any one of the Ru atoms would have about the same effect on the oxidation potential of the cluster.

Pi donor substituents on the allylidene unit have profound effects upon the cluster structure and electron density. Structural distortion of the Ru_3C_3 cluster core of (μ-H)Ru_3(μ_3-η^3-Me_2NCCHCMe)$(CO)_9$ has been attributed to pi donation by the amino substituent ([4]a). This distortion, involving lengthening of the bond between the amino-substituted allylidene carbon and the apical Ru atom, was termed a nido polyhedral distortion, as pi donation from the nitrogen atom has the effect of removing the allylidene carbon from the cluster core. Some limited electrochemical evidence of such pi donation has been provided [15].

We were interested in the effect of heteroatom substitution on the HOMO energy and charge localization. Fenske–Hall MO calculations were performed on (μ-H)Ru_3(μ_3-η^3-XCCRCR′)$(CO)_9$ (X = Me, R = R′ = Me; X = OMe, R = R′ = Me; X = NMe_2, R = H, R′ = Me), for which the accurate structural data are available ([4]a, [11]). The substituent dependence of the energy of the HOMO (-7.04, -6.90, and -6.63 eV, respectively) parallels the electrochemical data for the substituted analog (vide infra). The calculations also reveal that, while the total contributions of the basal Ru atoms to the HOMO remain relatively constant throughout the series, the contribution of the basal Ru atom adjacent to the heteroatom allylidene substituent increases with the pi donor character of the heteroatom (the contribution to the HOMO by orbitals of Ru(1), Ru(2), and Ru(3), respectively, in Fig. 1: 14, 14, and 33% for (μ-H)Ru_3(μ_3-η^3-MeCCMeCMe)$(CO)_9$; 16, 13, and 31% for (μ-H)Ru_3(μ_3-η^3-MeOCCMeCMe)$(CO)_9$; 21, 9, and 30% for (μ-H)Ru_3(μ_3-η^3-Me_2NCCHCMe)$(CO)_9$). Thus, the contributions from the two basal atoms to the HOMO are approximately equal for (μ-H)Ru_3(μ_3-η^3-MeOCCMeCMe)$(CO)_9$, but the basal Ru adjacent to the NMe_2 substituent makes a much larger contribution for (μ-H)Ru_3(μ_3-η^3-Me_2NCCHCMe)$(CO)_9$.

Crystallographic data are also available for other asymmetrical 1,3-dimetalloallyl clusters, including (μ-H)Ru_3(μ_3-η^3-MeCCMeCH)$(CO)_9$ [16], (μ-H)Ru_3(μ_3-η^3-MeCCHCH)$(CO)_{9-n}(PPh_3)_n$ [17], (μ-H)Ru_3(μ_3-η^3-Et_2NCCHCMe)$(CO)_8(PPh_3)$ [5] and (μ-H)Ru_3(μ_3-η^3-MeOCCMeCMe)$(CO)_7(PPh_3)_2$ [5]. The first and second PPh_3 substitutions, each on a different metal atom, are *cis* to the bridging hydride and the Ru–C sigma bond (Fig. 1); the structure of the metal–carbon core of these clusters is not affected by phosphine substitution [5,17].

3.2. Electrophilic addition

Electrophile/oxidants such as Ag^{1+} may either add to a metal–metal bond or oxidize the cluster. Electrophilic additions provide information concerning the charge distribution in organometallic clusters and, additionally, structural changes which sometimes accompany these additions can suggest structural changes which may occur upon oxidation of a 48-electron cluster. Electrophilic additions of protons and of Group 11 metals to metal clusters have attracted a great deal of attention; additions most commonly occur at a single metal-metal bond, but additions to trimetallic faces have also been reported [18]. Others have reported protonations of (μ-H)Ru_3(μ_3-η^3-MeCCHCMe)$(CO)_8(PPh_3)$ ([19]a) and (μ-H)Ru_3(μ_3-η^3-

$Me_2NCCHCMe)(CO)_8(PPh_3)$ ([19]b). To probe the reactivity of $HRu_3(\mu_3\text{-}\eta^3\text{-}XCCRCR')(CO_{9-n}(PPh_3)_n$ toward electrophilic addition/oxidation we examined reactions with $AgSO_3CF_3$, $Au(PPh_3)(SO_3CF_3)$, and trifluoroacetic acid.

Addition of $AgSO_3CF_3$ to a solution of $(\mu\text{-}H)Ru_3(\mu_3\text{-}\eta^3\text{-}MeOCCMeCMe)(CO)_7(PPh_3)_2$ produces a red solution, believed to contain the adduct $[(\mu\text{-}H)Ru_3(\mu_3\text{-}\eta^3\text{-}MeOCCMeCMe)(CO)_7(PPh_3)_2Ag][SO_3CF_3]$. The ^1H- and ^{31}P-NMR spectral data (see Section 2) are very similar to those of the neutral precursor. Since we were unable to further characterize this species, we investigated the corresponding reaction with $Au(PPh_3)SO_3CF_3$, which generally forms more stable adducts with metal clusters.

Treatment of the appropriate cluster with $AuPPh_3(SO_3CF_3)$ formed stable adducts $[(\mu\text{-}H)Ru_3(\mu_3\text{-}\eta^3\text{-}XCCRCR')(CO)_{9-n}(PPh_3)_nAuPPh_3][SO_3CF_3]$. NMR spectroscopy was particularly valuable in determining the regiochemistry of the electrophilic addition to the Ru_3C_3 skeleton. The $AuPPh_3$ moiety displays a ^{31}P resonance at ca. 60 ppm, with coupling to the resonance(s) due to the adjacent Ru-bound ^{31}P nuclei. The hydride bridging the same cluster edge as the allylidene displays coupling of 2 Hz to the central C–H and ca. 12 Hz to *cis*-PPh_3 ligands. The 3-methyl group displays a 3 Hz coupling to adjacent ^{31}P. The ^1H- and ^{31}P-NMR data are given in the Section 2. On these bases, the proposed structures were established.

The proposed structure for $[(\mu\text{-}H)Ru_3(\mu_3\text{-}\eta^3\text{-}Et_2NCCHCMe)(CO)_7(PPh_3)_2(AuPPh_3)][SO_3CF_3]$ is shown in Fig. 2. The ^{31}P-NMR spectrum displayed a resonance at 60.2 (d, 30 Hz) ppm due to the $AuPPh_3$ moiety, coupled to a resonance at 41.2 ppm, which is also coupled to the 3-methyl protons of the allylidene ligand. This suggests that the electrophilic addition of the gold moiety occurs at the Ru–Ru edge *syn* to the methyl substituent.

The structure proposed for $[(\mu\text{-}H)Ru_3(\mu_3\text{-}\eta^3\text{-}MeOCCMeCMe)(CO)_6(PPh_3)_3(AuPPh_3)][SO_3CF_3]$ is shown in Fig. 3. The very similar coupling constants between the three Ru-bound ^{31}P nuclei and the Au-bound ^{31}P nucleus (58.7 ppm (ddd, $J_{P-P} = 27$, 19, and 17 Hz) suggests that the Ru_3 face is capped by the Au atom.

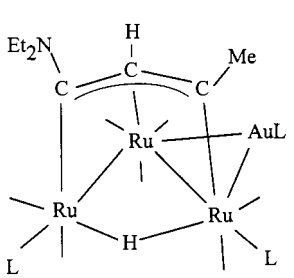

Fig. 2. Proposed structure for $[HRu_3(Et_2NCCHCMe)(CO)_7(PPh_3)_2(AuPPh_3)][SO_3CF_3]$.

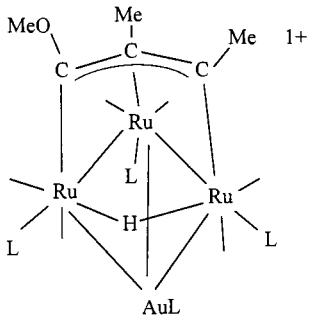

Fig. 3. Proposed structure for $[HRu_3(MeOCCMeCMe)(CO)_6(PPh_3)_3(AuPPh_3)][SO_3CF_3]$.

For $[(\mu\text{-}H)Ru_3(\mu_3\text{-}\eta^3\text{-}MeOCCMeCMe)(CO)_7(PPh_3)_2(AuPPh_3)][SO_3CF_3]$ only one isomer (I) was observed initially, but after 24 h a mixture of three isomers was observed by NMR spectroscopy. The proposed structures, displayed in Fig. 4, are based upon analysis of the NMR spectra. The similarity of the two ^{31}P–^{31}P coupling constants (see Section 2) to the $Au(PPh_3)$ moiety for each these isomers suggests that the $AuPPh_3$ moiety bridges the Ru_3 face, as proposed for the trisubstituted analog.

Study of electrophilic addition reactions was extended to protonation because of the isolobal relationship to the $AuPPh_3$ fragment [20]. Other workers previously reported protonations of *anti*-$(\mu\text{-}H)Ru_3(\mu_3\text{-}\eta^3\text{-}Et_2NCCHCMe)(CO)_8(PPh_3)$ ([19]b) and $(\mu\text{-}H)Ru_3(\mu_3\text{-}\eta^3\text{-}MeCCHCMe)(CO)_8(PPh_3)$ ([19]a); in these cases protonation occurs on the $(OC)_3Ru\text{–}Ru(CO)_2(PPh_3)$ bond and so no information concerning

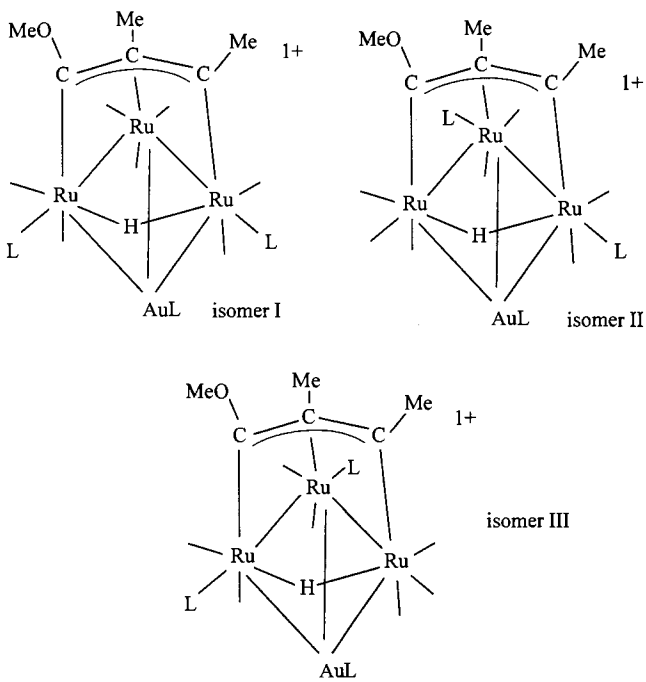

Fig. 4. Proposed structures for isomers $[HRu_3(MeOCCMeCMe)(CO)_7(PPh_3)_2(AuPPh_3)][SO_3CF_3]$.

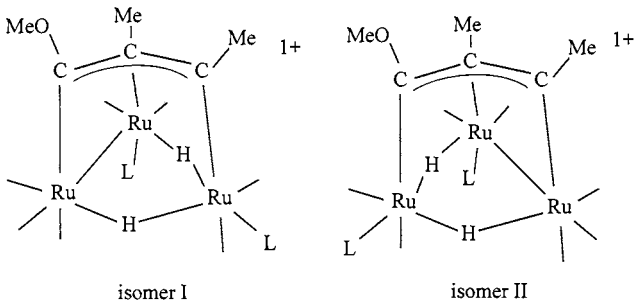

Fig. 5. Proposed structures for isomers $[H_2Ru_3(MeOCCMeCMe)(CO)_7(PPh_3)_2][O_2CCF_3]$.

the effect of the allylidene substituents on the HOMO is available. Protonations of $(\mu\text{-H})Ru_3(\mu_3\text{-}\eta^3\text{-Et}_2NCCHCMe)(CO)_7(PPh_3)_2$ and $(\mu\text{-H})Ru_3(\mu_3\text{-}\eta^3\text{-MeOCCMeCMe})(CO)_7(PPh_3)_2$ were performed by adding trifluoroacetic acid or trifluoromethanesulfonic acid directly to a solution in $CDCl_3$ in an NMR tube. The ^{1}H-NMR and ^{31}P-NMR data are given in the Section 2. Protonation of $(\mu\text{-H})Ru_3(\mu_3\text{-}\eta^3\text{-Et}_2NCCHCMe)(CO)_7(PPh_3)_2$ appears to occur at a basal Ru-apical Ru edge without structural isomerization. The regiochemistry of protonation cannot be determined unambiguously from these data. For $(\mu\text{-H})Ru_3(\mu_3\text{-}\eta^3\text{-MeOCCMeCMe})(CO)_7(PPh_3)_2$, the protonation reaction is more complicated. Two isomers $[(\mu\text{-H})_2Ru_3(\mu_3\text{-}\eta^3\text{-MeOCCMeCMe})(CO)_7(PPh_3)_2]^{1+}$ are formed; proposed structures are shown in Fig. 5. The initial product of protonation (isomer I) displays NMR data consistent with addition of the proton to a $Ph_3PRu–RuPPh_3$ edge which is adjacent to the edge bridged by the allylidene. Protonation induces a change in the phosphine substitutional distribution on the $Ru_3(C_3)$ core. After stirring for several hours under nitrogen in dichloromethane solution, a second isomer (II) is formed such that the equilibrium isomer I/isomer II ratio is 2:1. The singlet methyl resonance at 2.01 ppm indicates that the basal Ru atom *syn* to the 3-methyl group is not PPh_3 substituted.

3.3. Electrochemistry

A previous study of the electrochemistry of $(\mu\text{-H})Ru_3(\mu_3\text{-}\eta^3\text{-XCCHCMe})(CO)_9$ (X = Me, NMe_2) had found only irreversible oxidation processes. The authors had noted that the presence of the pi donor amino substituent reduced $E_{p,a}$ by 250 mV [15].

The electrochemical oxidations of the clusters $(\mu\text{-H})Ru_3(\mu_3\text{-}\eta^3\text{-XCCRCR}')(CO)_7(PPh_3)_2$ (X = NEt_2, R = H, R′ = Me; X = OMe, R = R′ = Me) were completely irreversible in acetonitrile, most likely because of the nucleophilic attack by the solvent on the oxidized species. For the monosubstituted clusters, the cyclic voltammetry for oxidation is also irreversible in dichloromethane. Anodic peak potentials at scan rates of 100 mV s^{-1} are given in Table 2. It is assumed that the irreversibility is due to a follow-up chemical reaction of the oxidized species.

In dichloromethane disubstituted and trisubstituted clusters exhibit in each case an electrochemically reversible or quasi-reversible oxidation, which is followed by a chemically irreversible oxidation at a more positive potential. Fig. 6 shows the cyclic voltammogram for $HRu_3(\mu_3\text{-}\eta^3\text{-Et}_2NCCHCMe)(CO)_7(PPh_3)_2$. Table 2 displays the electrochemical data for the cluster series $HRu_3(\mu_3\text{-}\eta^3\text{-XCCRCR}')(CO)_{9-n}(PPh_3)_n$, $n = 1, 2, 3$. Only the first oxidation process was studied in detail. Using the criteria of peak to peak separation ($\Delta E_p = 72$ mV for ferrocene/ferricenium in dichloromethane solution at 100 mV s^{-1}, assumed to be reversible) and peak current ratio ($i_{p,c}/i_{p,a} = 1$ for an chemically reversible process), it was determined that the first one-electron oxidation of $HRu_3(\mu_3\text{-}\eta^3\text{-XCCRCR}')(CO)_6(PPh_3)_3$ (X = MeO, R = H, R′ = EtO; X = MeO, R = Me, R′ = Me) was electrochemically reversible at a scan rate of 100 mV s^{-1}. All of the di-substituted clusters exhibited oxidation waves which were in the quasi-reversible regime. Both ΔE_p and the $i_{p,c}/i_{p,a}$ ratio increase with increasing scan rate. The increase in the $i_{p,c}/i_{p,a}$ ratio as the scan rate increases indicates that a follow-up chemical process causes decomposition of the radical cation. Based upon the identification of the decomposition product of $[HRu_3(\mu_3\text{-}\eta^3\text{-EtOCCHCOMe})(CO)_6(PPh_3)_3][SbCl_6]$ (vide infra) and upon our previous study of electrolyte-induced disproportionation of $[H_2Ru_3(XCCR)(CO)_6(PPh_3)_3]^{1+}$ [3], we propose that the radical cation product reacts with the electrolyte, causing cluster fragmentation.

In order to determine the number of electrons, n, involved in the first oxidation step, controlled potential coulometry was performed on $HRu_3(Et_2NCCHCMe)(CO)_7(PPh_3)_2$. This cluster was chosen for several reasons. The first oxidation wave was almost reversible based on ΔE_p and $i_{p,c}/i_{p,a}$, the oxidized product was found to be stable at room temperature for a few minutes and for about 1 h at low temperature (228–250 K), and the large separation between the first and second oxidation waves (> 400 mV) ensures that a potential could be chosen for the coulometry without interference from the second oxidation step. Controlled potential coulommetry yielded a value of 1.03 Faraday per mole for the first oxidation process.

3.4. Chemical oxidation

Radical cations were obtained preparatively by chemical oxidation. As described above, the 1,3-dimetalloallyl clusters appear to react with Ag^{1+} initially to form electrophilic addition products. These adducts are stable for long periods in dichloromethane in most cases. Only the Ag^+ adduct with $(\mu\text{-H})Ru_3(\mu_3$-

Table 2
Cyclic voltammetric data for $HRu_3(CXCRCR')(CO)_{9-n}(PPh_3)_n$ ($n = 1, 2, 3$) in dichloromethane

	$(E_{p,a}+E_{p,c})/2$ or $[E_{p,a}]$ (V)	ΔE_p (mV)	$i_{p,c}/i_{p,a}$	$E_{p,a2}$ (V)	Diffusion coefficient, D_R (10^{-6} cm^2 s^{-1})
syn-$HRu_3(Et_2NCCHCMe)(CO)_8$	[0.54]				6.3(0.4)
(PPh_3)					
anti-$HRu_3(Et_2NCCHCMe)(CO)_8$	[0.43]				6.6(0.4)
(PPh_3)					
syn-$HRu_3(MeOCC_2Me_2)(CO)_8(PPh_3)$	[0.58]				5.9(0.1)
anti-$HRu_3(MeOCC_2Me_2)(CO)_8(PPh_3)$	[0.59]				5.8(0.4)
$HRu_3(Et_2NCCHCMe)(CO)_7(PPh_3)_2$	0.09	75	0.88	0.51	5.8(0.6)
$HRu_3(MeOCC_2Me_2)(CO)_7(PPh_3)_2$	0.28	74	0.90	0.74	5.1(0.3)
$HRu_3(MeOCC_2Me_2)(CO)_6(PPh_3)_3$	0.02	70	0.95	0.47	4.8(0.2)
$HRu_3(MeOCCHCOEt)(CO)_7(PPh_3)_2$	0.18	72	0.89	0.56	4.74(0.12)
$HRu_3(MeOCCHCOEt)(CO)_6(PPh_3)_3$	−0.13	68	1.00	0.32	4.47(0.10)

10^{-3} M cluster in 0.1 M TBATFB in dichloromethane at 25°C, the working electrode was a 5 mm diameter platinum disk, the auxilary electrode and the reference electrode were a platinum wire and a silver wire, respectively. Scan rate was 100 mV s^{-1}. The potentials are referenced to the ferrocene/ferricenium couple (0 V, $\Delta E_p = 72$ mV) under the same conditions.

η^3-$Et_2NCCHCMe)(CO)_7(PPh_3)_2$ subsequently led to the oxidized species in minutes, indicated by a color change from red to dark green.

Radical cations could be obtained by oxidation with tris(4-bromophenyl)aminium hexachloroantimonate, 'magic blue'. The oxidation reactions for all these clusters exhibit an immediate color change upon addition of the 'magic blue'. For $HRu_3(Et_2NCCHCMe)(CO)_7(PPh_3)_2$, the color changed from orange/yellow to dark green immediately. For the other disubstituted clusters, $HRu_3(MeOCC_2Me_2)(CO)_7(PPh_3)_2$ and $HRu_3(MeOCCHCOEt)(CO)_7(PPh_3)_2$, the color of the oxidized solutions appeared to be yellow/green. The radicals decomposed at room temperature within several minutes, to give a yellow solution. In order to characterize the radical cations by spectroscopic methods and study the stability of the radical clusters, the oxidation reactions were also performed at −40°C. Low temperature IR and EPR spectra were recorded in dichloromethane.

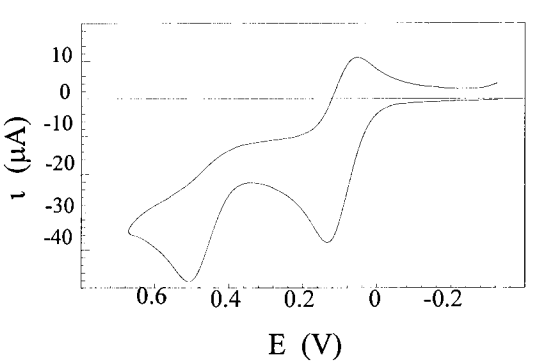

Fig. 6. Cyclic voltammogram for $HRu_3(Et_2NCCHCMe)(CO)_7(PPh_3)_2$.

An IR spectrum for each of the radical cations derived by oxidation of $HRu_3(XCCRCR')(CO)_{9-n}(PPh_3)_n$ (X = OMe, R = R′ = Me; X = OMe, R = H, R′ = OEt; X = NEt_2, R = H, R′ = Me; $n = 2, 3$) was obtained by recording the spectrum of the oxidized species in dichloromethane immediately after mixing the cluster solution and the oxidizing agent at −40°C. The CO stretching frequencies are shifted to a higher frequency for the radical cation in comparison to the parent cluster. The stabilities of these radical cations were monitored by taking IR spectra at 5–10 min intervals. IR data are presented in Table 1. The stabilities of the radical products were comparable to that of the alkylidyne cation radical $[H_3Ru_3(COMe)(CO)_7(PPh_3)_2]^{1+}$ at room temperature [2], and were greater than that of $[H_2Ru_3(\mu_3\text{-}\eta^2\text{-}XCCR)(CO)_7(PPh_3)_2]^{1+}$ [3]. All of the radical cations persisted for at least 1 h at low temperature. The radical derived from the tri-substituted derivative formed more readily than the di-substituted analog. $HRu_3(Et_2NCCHCMe)(CO)_7(PPh_3)_2$ was also oxidized rapidly by one equivalent of oxidant. However, for $HRu_3(MeOCC_2Me_2)(CO)_7(PPh_3)_2$ and $HRu_3(MeOCCHCOEt)(CO)_7(PPh_3)_2$, the radicals were not clearly identified in the IR spectrum immediately when one equivalent of oxidant was added. For example, the periodically recorded IR spectra of the oxidation product from $HRu_3(MeOCC_2Me_2)(CO)_7(PPh_3)_2$ showed the slow growth of a new peak at 2069 cm^{-1}, accompanied by decreasing intensities of the peaks at 2042 and 2001 cm^{-1}, assigned to the starting material. Furthermore, the decomposition of the radical cation cluster proceeded before all of the starting material was oxidized. A clean IR spectrum for the radical cluster could not be obtained due to the slow oxidation. Thus, it was necessary to use an excess amount of oxidant to

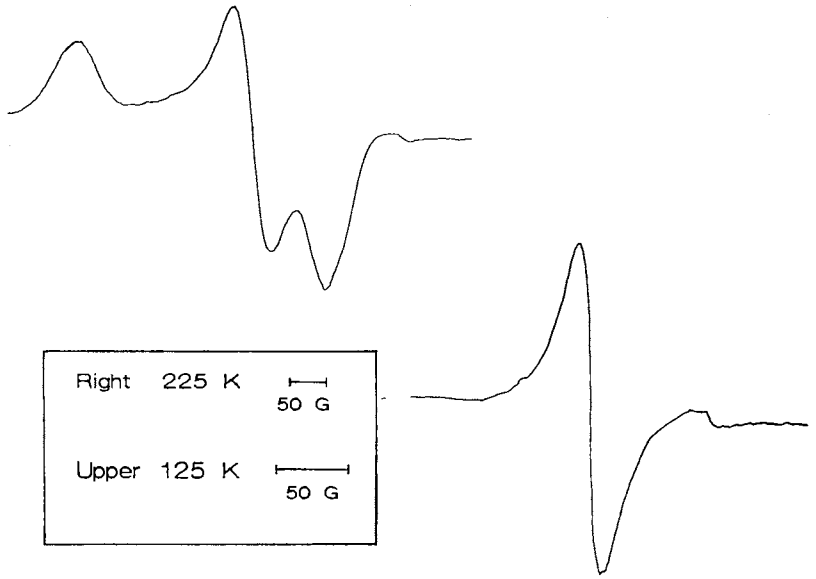

Fig. 7. EPR spectrum of $[HRu_3(Et_2NCCHCMe)(CO)_7(PPh_3)_2]^{1+}$ at 225 and 125 K in dichloromethane.

characterize the di-substituted radical cations by IR spectroscopy.

Available spectral data for the oxidation products provided no evidence concerning their composition, in particular whether the fragmentation occurred. To determine if the integrity of the precursor cluster was maintained, a follow-up reduction of the product of oxidation of $HRu_3(Et_2NCCHCMe)(CO)_7(PPh_3)_2$ was conducted. The IR spectrum at -40°C was recorded before oxidation, after oxidation with 'magic blue', and after the follow-up reduction with $HSnBu_3$. The peaks due to the oxidation product were greatly reduced upon the treatment with $HSnBu_3$, and the spectrum appeared to be mainly that of the starting material despite the presence of some minor side products. The ^{1}H-NMR spectrum of the oxidation–reduction solution also displayed signals due mainly to the starting material. This experiment suggests that the skeleton of the cluster is retained in its oxidized form.

After 1 h, the spectrum of each oxidized cluster system changed significantly, which was presumed to indicate decomposition of the compound. The decomposition of each radical cation at low temperature resulted in broad peaks in the IR spectra. No products were identified from the reactions.

3.5. Low temperature EPR spectra

Fig. 7 displays the EPR spectrum for $[HRu_3(Et_2NCCHCMe)(CO)_7(PPh_3)_2^1]^{+}$ in dichloromethane at 225 and 125 K (frozen solution). Generally, the EPR spectrum for each cluster radical in dichloromethane at 225 K displayed a singlet with a g value characteristic of a metal centered radical. In frozen solution the three components of the g tensor were resolved. A comparison of the g value of the singlet at 225 K with the average g value at 125 K is displayed in Table 3. The full width δ (G) between derivative extrema was also measured for each cluster at 225 K, and the results were displayed in Table 3. The trisubstituted cluster radicals appear to have broader EPR signals than the corresponding disubstituted radi-

Table 3
EPR data for $[HRu_3(XCCRCR')(CO)_{9-n}(PPh_3)_n]^{1+}$

In dichloromethane at 125 K			
Radical	g_1	g_2	g_3
$[HRu_3(Et_2NCCHCMe)(CO)_7(PPh_3)_2]^{1+}$	2.221	2.098	2.048
$[HRu_3(MeOCCHCOEt)(CO)_7(PPh_3)_2]^{1+}$	2.204	2.088	2.040
$[HRu_3(MeOCCHCOEt)(CO)_6(PPh_3)_3]^{1+}$	2.208	2.095	2.020
$[HRu_3(MeOCCMeCMe)(CO)_6(PPh_3)_3]^{1+}$	2.208	2.107	2.047
In dichloromethane at 125 and 225 K			
Radical	$<g>$ (125 K)	g (225 K)	δ (G)
$[HRu_3(Et_2NCCHCMe)(CO)_7(PPh_3)_2]^{1+}$	2.122	2.119	56.0
$[HRu_3(MeOCCHCOEt)(CO)_7(PPh_3)_2]^{1+}$	2.110	2.107	50.5
$[HRu_3(MeOCCHCOEt)(CO)_6(PPh_3)_3^{11}]^{+}$	2.108	2.106	66.8
$[HRu_3(MeOCCMeCMe)(CO)_6(PPh_3)_3]^{1+}$	2.120	2.115	73.9

cals. The EPR spectra for the radical cations $[H_3Ru_3(\mu_3\text{-CX})(CO)_{9-n}(PPh_3)_n]^{1+}$ (dichloromethane solution, g 2.06–2.09) displayed resolvable hyperfine coupling to phosphine ligands trans to the Ru–CX bonds (a{^{31}P} 2.6–6.0 mT) but not to *cis* ligands [2]. The δ values of $[HRu_3(XCCRCR')(CO)_{9-n}(PPh_3)_n]^{1+}$ are at least twice as large as those of the EPR signals of $[H_3Ru_3(\mu_3\text{-CX})(CO)_{9-n}(PPh_3)_n]^{1+}$. These phenomena suggest the presence of unresolved hyperfine coupling to the ^{31}P nuclei in the EPR spectra of $[HRu_3(XCCRCR')(CO)_{9-n}(PPh_3)_n]^{1+}$.

4. Discussion

Ligand additivity, the concept that ligand effects upon a transition metal center are additive, is a well-established phenomenon for substituted mononuclear complexes, for which the HOMO usually has dπ character [21]. Correlations of oxidation potentials with substituent effects and with HOMO energies have been noted by many of workers. A number of parameter sets have been developed to correlate various properties of metal complexes with the steric and electronic properties of ligands such as tertiary phosphines. Lever has established a set of ligand parameters E_L based upon an extensive compilation of oxidation potentials for octahedral Ru(II)/Ru(III) mononuclear complexes ([22]a). This ligand parameter set allows the prediction of the $E_{1/2}$ for any given octahedral mononuclear Ru(II) complex and has been extended to other monometallic complexes ([22]b,c). The application of Lever's parameters to the electrochemistry of $[Ru_3(\mu_3\text{-O})(OAc)_6L_3]^n$ ($n = -1$ to $+2$) was studied by Toma [23]; this compound, which is a 51-e cluster in the $+1$ state, differs from the clusters described below because the HOMO is not associated with the organometallic cluster bonding framework.

Ligand additivity in metal cluster systems has not been investigated in a systematic manner, although ligand effects upon cluster electron densities have been reported in many systems. Since the HOMO of a metal cluster is commonly a metal-metal bonding orbital, there seems to be no good reason to expect that metal clusters should show the same degree of ligand additivity as mononuclear metal complexes. Furthermore, when the HOMO does not contain equal contributions from all the metal atoms in the cluster, one would reasonably expect that the regiochemistry of ligand substitution would influence the oxidation potential (as well as the stability of the radical cation product).

We recently reported an analysis of the ligand and substituent effects upon the oxidation potential of the series $H_3Ru_3(\mu_3\text{-CX})(CO)_{9-n}L_n$ using Lever's parameterized equation, modified with a Hammet term [24] to account for the alkylidyne substituent (Eq. (1), $n = 1$) ([2]c). Here, we adopt the terminology of Bursten that 'ligand effects' refer to effects due to the steric and electronic properties of the ligand directly bonded to a metal center (e.g. CO versus PPh_3), whereas 'substituent effects' are effects due to the steric and electronic properties of substituents of organic moieties remote from the metal center (e.g. substituents on the hydrocarbyl fragment) [21]. For this cluster series the HOMO has Ru–CX bonding character, involving all three Ru atoms [2]. An excellent correlation ($S_{M_3} = 0.37(0.03)$, $\rho = 6.0(0.7)$, and $I_{M_3} = -2.5(0.2)$ V, correlation 0.962) was obtained, involving significant ligand and substituent effects upon the oxidation potential, with oxidation potentials ranging over 1 V.

$$E_{\text{observed}}\,(\text{V}) = S_{M_3}\sum_{i=1}^{9} E_L(L_i) + 2.303(RT/nF)\rho\sum_{i=1}^{n}\sigma_p^+(X_i) + I_{M_3} \quad (1)$$

The electrochemistry of the series $HRu_3(\mu_3\text{-}\eta^3\text{-XCCRCR}')(CO)_{9-n}(PPh_3)_n$ provides additional insight into ligand additivity and substituent effects in cluster systems. Unlike the series we studied previously, the HOMO has metal–metal bonding character, with the primary contribution from the apical Ru (ca. 30%), which is η^3-bonded to the allylidene ligand, and significant contributions from the two basal Ru atoms. While we are unable to achieve a series of clusters (Table 4) having a large range of substituent (σ_p^+ -1.40 to

Table 4
$E_{p,a}$, ligand and substituent parameters

	Compound	$E_{p,a}$ (V)	ΣE_L	$\Sigma \sigma_p^+$
1	*syn*-$HRu_3(Et_2NCCHCMe)(CO)_8(PPh_3)$	0.54	8.31	−2.38
2	*anti*-$HRu_3(Et_2NCCHCMe)(CO)_8(PPh_3)$	0.43	8.31	−2.38
3	*syn*-$HRu_3(MeOCC_2Me_2)(CO)_8(PPh_3)$	0.58	8.31	−1.4
4	*anti*-$HRu_3(MeOCC_2Me_2)(CO)_8(PPh_3)$	0.59	8.31	−1.4
5	$HRu_3(Et_2NCCHCMe)(CO)_7(PPh_3)_2$	0.13	7.71	−2.38
6	$HRu_3(MeOCCMeCMe)(CO)_7(PPh_3)_2$	0.32	7.71	−1.4
7	$HRu_3(MeOCC_2Me_2)(CO)_6(PPh_3)_3$	0.05	7.11	−1.4
8	$HRu_3(MeOCCHCOEt)(CO)_7(PPh_3)_2$	0.22	7.71	−1.59
9	$HRu_3(MeOCCHCOEt)(CO)_6(PPh_3)_3$	−0.10	7.11	−1.59

Ligand parameters ([22]a): CO (0.99), PPh_3 (0.39).
Substituent parameters [24]: OMe (−0.78), OEt (−0.81), NEt_2, (−2.07), Me (−0.31).

-2.38) or ligand parameters (ΣE_L 7.11 to 8.31), this series does allow for variation in the regiochemistry of ligand substitution. Electrochemical 1-electron oxidation of $HRu_3(\mu_3\text{-}\eta^3\text{-}XCCRCR')(CO)_{9-n}(PPh_3)_n$ ($n = 2$ or 3) is a kinetically facile process. As the oxidations of the monosubstituted clusters are irreversible, we have used for comparison the anodic peak potentials as determined by cyclic voltammetry at 100 mV s^{-1}. It should be noted that $(E_{p,a} - E_{1/2})$ will increase as the couple becomes more irreversible, and, therefore, comparisons of data for the quasi-reversible and irreversible examples should be viewed with caution. Also, we have a very limited variety of ligand and substituent types. Nonetheless a good fit (Fig. 8) of the observed anodic peak potentials (at 100 mV s^{-1}) can be made to Eq. (1). Here the ligand parameters E_L are summed over the 9 CO or PPh_3 ligands of the triruthenium core and the substituent parameters are summed over the three ($n = 3$) allylidene substituents X_i. A non-linear least-squares fit of the data to Eq. (1) (correlation 0.981) yielded values of $S_{M_3} = 0.52(0.04)$, $\rho = 2.3(0.8)$, and $I_{M_3} = -3.5(0.3)$ V. The fit is actually slightly better if only the allylidene substituents on the terminal carbons are used ($S_{M_3} = 0.51(0.04)$, $\rho = 1.9(0.5)$, and $I_{M_3} = -3.5(0.3)$ V, correlation 0.985), but as only methyl and hydrogen have been used as central carbon substituents, the significance of this observation is not clear. However, since the contributions of the orbitals of the terminal carbon atoms to the HOMO are much greater than the contributions due to the central atom, this may suggest that the 1- and 3-substituents have a greater effect on the HOMO. The constant I_{M_3} serves to scale the potential to a hypothetical complex $HRu_3(\mu^3\text{-}\eta^3\text{-}HCCHCH)L_9$ where $E_L(L) = 0$ and corrects for differences in reference potentials (Lever's E_L parameters are based upon the NHE reference, whereas we are using ferrocene/ferricenium = 0 V).

The second term in Eq. (1) represents the effect of the allylidene substituents upon the oxidation potential. The substituent parameter set σ_p^+ is derived for substituents which can delocalize positive charge by conjugation. An essentially equivalent correlation is obtained using the parameter set R^+ ($S_{M_3} = 0.45(0.04)$, $\rho = 8.4(2.6)$, and $I_{M_3} = -2.8(0.3)$ V, correlation 0.982); this set, derived from σ_p^+, is primarily for resonance effects. A substantially poorer fit is obtained with the parameter set σ_p ($S_{M_3} = 0.52(0.06)$, $\rho = 3.4(1.8)$, and $I_{M_3} = -3.6(0.4)$ V, correlation 0.970). Although only a few substituents are available, it is clear that pi conjugation is necessary to account for the reduction in oxidation potential caused by the NEt_2 substituent. This conclusion has been drawn previously from electrochemical [15] and structural [5] studies. The substituent coeffecient for the series $H_3Ru_3(\mu_3\text{-}CX)(CO)_{9-n}(L)_n$ ($\rho = 6.0(0.7)$) is substantially larger than that for $HRu_3(\mu_3\text{-}\eta^3\text{-}XCCRCR')(CO)_{9-n}(PPh_3)_n$ ($\rho = 2.3(0.8)$); this perhaps is due to the fact that the HOMO for the former is associated with Ru–CX bonding and the HOMO for the latter is associated with Ru–Ru bonding.

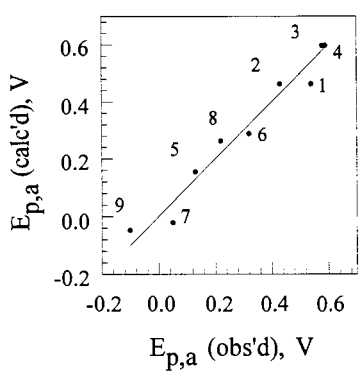

Fig. 8. Plot of $E_{p,a}$ (observed) versus $E_{p,a}$ (calculated) from Eq. (1), where $S_{M_3} = 0.52(0.04)$, $\rho = 2.3(0.8)$, and $I_{M_3} = -3.5(0.3)$ V. Numerals correspond to entries in Table 4.

The first term in Eq. (1) represents the effect of phosphine substitution for CO upon the oxidation potential of the cluster. The coefficient S for a mononuclear Ru(II)/Ru(III) couple is ideally 1. The observation that S_{M_3} for these triruthenium clusters is 0.52 and that the oxidation potentials for the entire series fit the same equation, with little or no dependence upon the regiochemistry of PPh_3 substitution, suggest that ligand additivity on a cluster core is as valid as for mononuclear complexes, i.e. a substituent on the entire cluster core affects the HOMO energy in the same way that ligand substitution on a mononuclear complex affects the 4d orbitals of a single Ru(II) atom, but with a reduction in magnitude as the ligand effects are distributed over more metal atoms. The ligand coefficients S_{M_3} for $H_3Ru_3(\mu_3\text{-}CX)(CO)_{9-n}(L)_n$ (0.37) and for $HRu_3(\mu_3\text{-}\eta^3\text{-}XCCRCR')(CO)_{9-n}(PPh_3)_n$ are quite similar, perhaps suggesting that Ru_3 clusters may be treated to a reasonable degree of accuracy with a common ligand coefficient. Obviously, more study is required to assess the validity of this treatment.

It is surprising that the regiochemistry of substitution has such a small effect. We expected that the largest effect upon the oxidation potential would be found for substitution at the Ru atom which makes the largest contribution to the HOMO, the Ru atom which is bound in an η^3-fashion to the hydrocarbyl ligand. However, the trisubstituted clusters have oxidation potentials only slightly lower than those predicted by best-fit correlation for the entire series. Also, for $HRu_3(Et_2NCCHCMe)(CO)_9$ the contributions to the HOMO from the two basal Ru atoms bridged by the hydride are very different, with Ru (1) *syn* to the amino substituent contributing 21% and Ru(2), 9%. Therefore, it was expected that *syn* substitution by PPh_3 would lower the oxidation potential to a greater extent than

anti substitution. However, the anodic peak potential for *anti*-$HRu_3(Et_2NCCHCMe)(CO)_8(PPh_3)$ is 110 mV lower than that of the *syn* isomer. The anodic peak potentials of the two isomers of $HRu_3(MeOCC_2Me_2)(CO)_8(PPh_3)$ are almost the same, but since the theoretical calculation shows that contributions to the HOMO of $HRu_3(MeOCC_2Me_2)(CO)_9$ from the two basal Ru atoms bridged by the hydride are approximately equal [7], this is perhaps to be expected.

The isolobal relationship between organometallic clusters and pi-hydrocarbon complexes is well-established. By this relationship, the clusters $HRu_3(\mu_3\text{-}\eta^3\text{-}XCCRCR')(CO)_{9-n}(PPh_3)_n$ are analogous to $(\eta^5\text{-}Cp)RuL_3^{1+}$ complexes. The oxidation potentials of $Cr(\eta^6\text{-}C_6H_5X)(CO)_3$ [25] and $Fe(\eta^5\text{-}C_5H_4X)Cp$ [26] have been previously correlated with σ_I and σ_p, respectively. The non-linear least squares fits of the published oxidation potentials for $Cr(\eta^6\text{-}C_6H_5X)(CO)_3$ and for $Fe(\eta^5\text{-}C_5H_4X)Cp$ with ring substituent constants σ_p^+ yield $\rho = 3.8(0.3)$ (correlation 0.981) and 5.2(0.4) (correlation 0.975), respectively [2]. The σ_p^+ value for $HRu_3(\mu_3\text{-}\eta^3\text{-}XCCRCR')(CO)_{9-n}(PPh_3)_n$, while somewhat smaller than these, is still very significant.

One-electron oxidation potentials very commonly track with Lewis basicities. We had thought that the regiochemistry of Lewis acid addition might shed light upon the charge densities in the HOMOs of these asymmetrically substituted clusters. On the basis of the Fenske–Hall calculations, electrophilic additions to metal–metal bonds of the bis- and tris-phosphine substituted clusters are expected to occur most favorably *syn* to the pi donor hydrocarbyl substituents. This regiochemical preference should be stronger for the stronger pi donating substituents. This is contrary to what is observed for addition of $Au(PPh_3)^{1+}$ to $HRu_3(\mu_3\text{-}\eta^3\text{-}Et_2NCCHCMe)(CO)_7(PPh_3)_2$, which occurs across the Ru–Ru bond which is *syn* to the Me substituent and without any structural isomerization. Addition of H^{1+} to $HRu_3(\mu_3\text{-}\eta^3\text{-}MeOCCMeCMe)(CO)_7(PPh_3)_2$ most likely occurs at a basal Ru-apical Ru edge and causes PPh_3 positional isomerization. Addition of $Au(PPh_3)^{1+}$ to $HRu_3(\mu_3\text{-}\eta^3\text{-}MeOCCMeCMe)(CO)_7(PPh_3)_2$ and $HRu_3(\mu_3\text{-}\eta^3\text{-}MeOCCMeCMe)(CO)_6(PPh_3)_3$ appears to occur across the Ru_3 face and again induces PPh_3 positional isomerization. The diversity of the modes of electrophilic addition makes it problematic to correlate the oxidation potentials of these clusters with the electrophilic addition products.

5. Conclusions

(1) The HOMO for $HRu_3(\mu_3\text{-}\eta^3\text{-}XCCRCR')(CO)_{9-n}(PPh_3)_n$ is metal–metal bonding in character, involving all three Ru atoms. The main contribution comes from the apical Ru, and there is an increasing contribution from the basal Ru *syn* to the pi-donor allylidene substitutent, at the expense of the other basal Ru atom, as the pi donor ability increases.

(2) Even though the three Ru atoms make unequal contributions to the HOMO the oxidation potential can be treated by ligand additivity for the entire Ru_3 cluster core. Ligand additivity on a cluster core is as valid as for mononuclear complexes, i.e. a substituent on the entire cluster core affects the HOMO energy in the same way that ligand substitution on a mononuclear complex affects the 4d orbitals of a single Ru(II) atom, but with a reduction in magnitude as the ligand effects are distributed over more metal atoms.

(3) Electrophilic addition of Ag^+ and AuL^+ to the Ru_3 core is kinetically favored over 1-e oxidation, and the regiochemistry of electrophilic addition does not always reflect the concentration of electon density in the HOMO.

(4) A new class of 47-e cluster radicals, $[HRu_3(\mu_3\text{-}\eta^3\text{-}XCCRCR')(CO)_{9-n}(PPh_3)_n]^{1+}$, has been prepared; this class is significantly less stable, for clusters of comparable oxidation potentials, than $[H_3Ru_3(\mu_3\text{-}CX)(CO)_{9-n}(PPh_3)_n]^{1+}$, for which the SOMO has metal-carbon bonding character, but more stable than $[H_2Ru_3(\mu_3\text{-}\eta^2\text{-}XCCR)(CO)_{9-n}(PPh_3)_n]^{1+}$, for which the SOMO is associated with a single Ru–Ru bond.

Acknowledgements

This work was supported by the National Science Foundation through Grant CHE-9213695 (JBK). The $\{^{31}P\}^1H$-NMR spectrum were kindly provided by Dr Sunil-Dutta Soni of Varian Associates, Florham Park, NJ.

References

[1] (a) D. Astruc, Electron Transfer and Radical Processes in Transition-Metal Chemistry, VCH, New York, 1995. (b) W.C. Trogler (Ed.), Organometallic Radical Processes, Elsevier, Amsterdam, 1990. (c) D.H. Evans, Chem. Rev. 90 (1990) 739. (d) J.K. Kochi, J. Organomet. Chem. 300 (1986) 139. (e) D.R. Tyler, Prog. Inorg. Chem. 36 (1988) 125. (f) N.G. Connelly, Chem. Soc. Rev. 18 (1989) 153. (g) W.E. Geiger, Prog. Inorg. Chem. 33 (1985) 275. (h) A.E. Stiegman, D.R. Tyler, Comments on Inorganic Chemistry 5 (1986) 215.

[2] (a) W.G. Feighery, R.D. Allendoerfer, J.B. Keister, Organometallics 9 (1990) 2424. (b) W.G. Feighery, Ph. D. Thesis, State University of New York at Buffalo, 1990. (c) W.G. Feighery, H. Yao, A.F. Hollenkamp, R.D. Allendoerfer, J.B. Keister, Organometallics 17 (1998) 872.

[3] W. Paw, C.H. Lake, M.R. Churchill, J.B. Keister, Organometallics, 14 (1995) 3768.

[4] (a) M.R. Churchill, L.A. Buttrey, J.B. Keister, J.W. Ziller, T.S. Janik, W.S. Striejewske, Organometallics 9 (1990) 766. (b) A.

Cox, P. Woodward, J. Chem. Soc. A (1971) 3599. (c) B.E. Hanson, B.F.G. Johnson, J. Lewis, P.R. Raithby, J. Chem. Soc., Dalton Trans. (1980) 1852. (d) S. Aime, A. Tiripicchio, M.T. Camellini, A.J. Deeming, Inorg. Chem. 20 (1981) 2027. (e) S. Aime, D. Osella, A.J. Deeming, A.J. Arce, M.B. Hursthouse, H.M. Dawes, J. Chem. Soc., Dalton Trans. (1986) 1459.

[5] M.R. Churchill, C.H. Lake, R.A. Lashewycz-Rubycz, H. Yao, R.D. McCargar, J.B. Keister, J. Organometal. Chem. 452 (1993) 151.

[6] P. Brun, P. Vierling, J.G. Riess, G. Le Borgne, Organometallics 6 (1987) 1032.

[7] (a) H. Yao, R.D. McCarger, R.D. Allendoerfer, J.B. Keister, Organometallics 12 (1993) 4283. (b) R.D. McCarger, M.A. Thesis, State University of New York at Buffalo, 1991. (c) H. Yao, Ph.D. Thesis, State University of New York at Buffalo, 1994.

[8] (a) F.G. Mann, A.F. Wells, D. Purdie, J. Chem. Soc. (1937) 1828. (b) C. Kowala, J.M. Swan, Aust. J. Chem. 19 (1966) 547.

[9] W.E. Geiger, in: J.J. Zuckerman (Ed.), Inorganic Reactions and Methods, vol. 15, VCH, Deerfield Beach, FL, 1986, p. 88.

[10] M.B. Hall, R.F. Fenske, Inorg. Chem. 11 (1972) 768.

[11] G. Granozzi, E. Tondello, R. Bertoncello, S. Aime, D. Osella, Inorg. Chem. 24 (1985) 570.

[12] J.W. Richardson, M.J. Blackman, J.E. Ranochak, J. Chem. Phys. 58 (1973) 3010.

[13] (a) E. Clementi, J. Chem. Phys. 40 (1964) 1944. (b) E.J. Clementi, IBMJ. Res. Dev. 9 (1965) 2.

[14] R.F. Fenske, D.D. Radtke, Inorg. Chem. 7 (1968) 479.

[15] P. Zanello, S. Aime, D. Osella, Organometallics 3 (1984) 1374.

[16] C. Jangala, E. Rosenberg, D. Skinner, S. Aime, L. Milone, E. Sappa, Inorg. Chem. 19 (1980) 1571.

[17] K.M. Rao, R.J. Angelici, V.G. Young, Jr., Inorg. Chim. Acta 198–200 (1992) 211.

[18] I.D. Salter, Adv. Organometal. Chem. 29 (1989) 249, and references therein.

[19] (a) E. Rosenberg, D.M. Skinner, S. Aime, R. Gobetto, L. Milone and D. Osella, Gazzetta Chimica Italiana 121 (1991) 313. (b) S. Aime, G. Jannon, D. Osella, A.J. Deeming, J. Organometal. Chem., 214 (1981) C15.

[20] D.G. Evans, DM.P. Mingos, J. Organometal. Chem. 232 (1982) 171.

[21] B.E. Bursten, M.R. Green, Prog. Inorg. Chem. 36 (1988) 393, and references therein.

[22] (a) A.B.P. Lever, Inorg. Chem. 29 (1990) 1271. (b) A.B.P. Lever, Inorg. Chem. 30 (1991) 1980. (c) E.S. Dodsworth, A.A. Vlcek, A.B.P. Lever, Inorg. Chem. 33 (1994) 1045.

[23] A.D.P. Alexiou, H.E. Toma, J. Chem. Res. (S) (1993) 464.

[24] C. Hansch, A. Leo, R.W. Taft, Chem. Rev. 91 (1991) 165.

[25] A.D. Hunter, V. Mozol, S.D. Tsai, Organometallics 11 (1992) 2251.

[26] W.E. Britton, R. Kashyap, M. El-Hashash, M. El-Kady, M. Herberhold, Organometallics 5 (1986) 1029, and references therein.